Monthly Notices
of the
ROYAL ASTRONOMICAL SOCIETY

Mon. Not. R. Astron. Soc. **402,** 575–588 (2010) doi:10.1111/j.1365-2966.2009.15910.x

A search for southern ultracool dwarfs in young moving groups

J. R. A. Clarke,[1⋆] D. J. Pinfield,[1] M. C. Gálvez-Ortiz,[1] J. S. Jenkins,[2] B. Burningham,[1] N. R. Deacon,[3,4] H. R. A. Jones,[1] R. S. Pokorny,[5] J. R. Barnes[1] and A. C. Day-Jones[1,2]

[1]*Centre For Astrophysics Research, University of Hertfordshire, College Lane, Hatfield, Hertfordshire AL10 9AB*
[2]*Department of Astronomy, Universidad de Chile, Casilla Postal 36D, Santiago, Chile*
[3]*Department of Astrophysics, Faculty of Science, Radboud University Nijmegen, PO Box 9010, 6500 GL Nijmegen, the Netherlands*
[4]*Institute for Astronomy, University of Hawaii, 2680 Woodlawn Drive, Honolulu, HI 96822, USA*
[5]*Yunnan Observatory, PO Box 110, CAS, 650011 Kunming, China*

Accepted 2009 October 20. Received 2009 October 19; in original form 2009 September 8

ABSTRACT

We associate 132 low-mass ultracool dwarfs in the southern hemisphere as candidate members of five moving groups (MGs) using photometric and astrometric selection techniques. Of these objects, we present high-resolution spectroscopy for seven candidates and combine these with previous measurements from the literature to determine spectral types and radial velocities. We thus constrain distance and space motion spectroscopically, allowing the kinematic membership of the MGs to be assessed. Possible membership of MGs has allowed ages and metallicities to be constrained for these objects and evolutionary models have been used to estimate their mass. We estimate that up to ∼75 of our candidate MG members should be genuine, and discuss future work that will confirm and exploit this major new sample.

Key words: stars: kinematics – stars: low-mass, brown dwarfs.

1 INTRODUCTION

Moving group (MG) populations are distinguishable from the field by their astrometric properties. An MG remains kinematically distinct within the general field population at ages ∼1 Gyr, before being dispersed by disc heating mechanisms (e.g. De Simone, Xiaoan & Tremaine 2004). MG populations are thought to originate in the same formation environment as open clusters. As the progenitor gas is cleared by OB star winds and the natal cluster expands, stars with sufficiently high velocities become unbound and form a young, coeval MG, possibly leaving behind a bound open cluster (Kroupa, Aarseth & Hurley 2001), before dispersal after up to ∼1 Gyr. MGs therefore consist of young populations with characteristic space motions, and membership of such groups can be used to constrain the age and composition of members.

A great deal of early work studying MGs was done by Eggen (e.g. Eggen 1958). Although many of the older groups identified in Eggen's work have since been shown to be spurious (e.g. Taylor 2000), with their velocity structure having other causes (e.g. the effects of stochastic spiral waves; Nordström et al. 2004), a variety of studies have shown that in general, the younger MGs are consistent with coeval populations of uniform metallicity (e.g. Soderblom & Mayor 1993; Feltzing & Holmberg 2000; Montes et al. 2001; King et al. 2003; King & Schuler 2005; De Silva et al. 2006).

⋆E-mail: j.r.a.clarke@herts.ac.uk

Ultracool dwarfs include objects with spectral type ≥M7. For the late M dwarfs (Jones & Tsuji 1997), atmospheric dust formation has important effects on opacity and general properties. The later T dwarf spectra are dominated by strong methane and water absorption (Burgasser et al. 2002). Ultracool dwarf masses are dependent on age, due to their significant luminosity and $T_{\rm eff}$ evolution, and they include both stellar and substellar (mass <0.075 $M_{\odot}$; Baraffe et al. 1998) objects.

The identification of ultracool dwarfs in MGs facilitates a variety of interesting areas of astronomical study.

(i) Ultracool MG members will provide excellent test-beds (with known age and metallicity) with which to improve our theoretical understanding of low-temperature and low-gravity dusty atmospheres. Such an understanding is a major stepping stone to properly characterizing local low-mass populations (via spectroscopic fitting), and thus measuring the low-mass/substellar initial mass function and formation history (see Pinfield et al. 2006).

(ii) Nearby intrinsically faint young stars facilitate particularly sensitive searches for binary companions over a large range of separation and mass ratios. Studies of the properties of low-mass binary systems (Guenther et al. 2001; Delgado-Donate et al. 2004; Luhman 2004; Feigelson et al. 2006) are vital to our understanding of dynamical processes that could be important in their formation (e.g. Whitworth & Stamatellos 2006).

(iii) Close low-mass binary systems in MGs could yield dynamical mass measurements, which could be used to test evolutionary models of low-mass stars and substellar objects (Kenworthy et al.

2001; Ribas 2003; Luhman, McLeod & Goldenson 2005; Pinfield, Jones & Steele 2005), providing a test for our understanding of their interior physics.

(iv) The youth and potential proximity of MG members could also allow one to search for planetary companions (e.g. Chauvin et al. 2004; see also Zuckerman et al. 2001; Nakajima et al. 2005) via adaptive optics (AO) techniques (e.g. Biller et al. 2006). Around young systems, giant planets will be brighter, and can be studied at relatively early evolutionary time (see Zuckerman & Song 2004). Furthermore, the intrinsic faintness of ultracool dwarfs reduce the contrast ratio for AO imaging at close separation (caused by the point-spread function of the primary). In essence, one can probe for lower mass planets around fainter dwarf hosts.

Recent work (e.g. Montes et al. 2001; López-Santiago et al. 2006) has produced some major new samples of nearby stars in MGs, in the early-F to M spectral type range. However, the number of ultracool dwarfs associated with MGs is still limited to a handful of objects (Ruiz, Takamiya & Roth 1991; Ribas 2003; Bannister & Jameson 2005; Barrado Y Navacués 2006; Kirkpatrick et al. 2006).

In this paper, we present the first stages of our new search for ultracool dwarfs in MGs in the solar neighbourhood. In the first part of the paper, we focus on the creation of our red object catalogue from which MG candidates will be selected (Section 2), and describe the astrometric and photometric selection techniques with which we identify our MG candidates (Section 3). We then discuss new radial velocities and space motions in the context of kinematic membership in Section 4 and provide a first-pass assessment of the credence of our MG candidates, describing how spectroscopic methods can further constrain the membership of the objects, providing examples. Section 5 gives a summary and discusses our planned future work with our new candidates.

2 HIGH PROPER MOTION RED OBJECT CATALOGUE

2.1 Proper motion catalogues

Large area proper motion surveys generally search for proper motions >0.4–0.5 arcsec yr^{-1} (Lépine, Shara & Rich 2002; Scholz et al. 2002; Deacon, Hambly & Cooke 2005; Lépine 2005; Subasavage et al. 2005), and are biased towards finding nearby and high-velocity objects. A survey over a greater range of proper motions and with good sensitivity to red objects would be more suitable for our purposes here.

The Liverpool–Edinburgh High Proper Motion Survey (LEHPM) of Pokorny, Jones & Hambly (2003) and Pokorny et al. (2004) covers proper motions >0.18 arcsec yr^{-1}, and was produced using SuperCOSMOS digitized *R*-band European Southern Observatory (ESO) and UK Schmidt plates. However, the frequency of spurious faint proper motion detections (due to various plate defects such as grains, bubbles in the emulsion, dust specks and scratches) requires a magnitude limit that is significantly brighter than the Schmidt plate limits. The LEHPM is limited to $R \sim 19.5$, which is quite restrictive when searching for red faint objects.

The Two Micron All Sky Survey (2MASS) can be brought to bear directly on these issues, both by providing an extra epoch to aid the removal of spurious proper motion objects, and also to provide optical near-infrared (IR) colours with which to select red objects.

We used two sources to compile our high proper motion red object catalogue. The first of these represents an extension of the LEHPM catalogue (which we refer to as ELEHPM), and is focused on obtaining a good accuracy for the proper motions using the large baselines available between the *R*-band Schmidt plate epochs. However, an expanded proper motion range (to >0.1 arcsec yr^{-1}) and a much deeper magnitude limit of $R = 21$ is used. The proper motions were derived using the same methods of Pokorny et al. (2003), and as expected, the initial optical list contained a very large number of spurious objects. These were dealt with to a large extent using an additional 2MASS epoch (see the next section). To compliment this *R*-band limited sample, we also selected from the Southern Infrared Proper Motion Survey (SIPS) catalogue (Deacon et al. 2005; Deacon & Hambly 2007). This catalogue suffers in part from short-time base lines (giving less accurate proper motions), but is *I*-band limited ($I = 18$) and thus photometrically more sensitive to very red objects than our *R*-band limited sample. We selected objects from both catalogues where $\mu/\Delta\sigma_\mu > 4$ (μ is proper motion and σ_μ is the proper motion one sigma uncertainty) to ensure our desired level of proper motion accuracy.

There is some overlap between the two samples, but it is not as significant as might be thought. 16 candidates appear in both the ELEHPM and SIPS but with proper motions that are in agreement (to 1σ). The SIPS objects have somewhat incomplete coverage due to proper motion uncertainties above our limit resulting from the shorter available SIPS baselines. Where the proper motions are accurate enough, however, the SIPS sensitivity probes more deeply for very red objects like L dwarfs.

We have also assessed the work of Faherty et al. (2009) who found that six of the SIPS objects have discrepancies with other catalogues. We instead use these proper motions when compiling our red object catalogue.

2.2 2MASS cross-match and colour cuts

We visually checked the SIPS catalogue and found it to be free of spurious objects, however our *R*-band limited sample was initially heavily contaminated. Many of these spurious sources could be removed by requiring an additional epoch detection in the 2MASS data base.

The epoch span of the optical and 2MASS measurements cover baselines of up to 25 yr. So, to cross-match the sources, the optical objects' proper motion was taken into account to derive the expected 2MASS coordinates. For each expected 2MASS position, we defined a search radius to account for uncertainties in this position. The size of the search radius depended on the accuracy of the SuperCOSMOS/2MASS coordinates, the epoch difference and the uncertainty associated with the proper motion, with typical search radii of $\sim$5 arcsec.

Colour cuts requiring $J - K_s \geq 1.0$ and $R - K_s \geq 5.0$ were also employed using the structured query language (SQL) interface of the 2MASS Gator, to ensure that objects with a spectral type predominantly later than M6 were returned (e.g. Kirkpatrick et al. 1999). We also required $J \leq 16$ (to avoid matches with very low signal-to-noise ratios (S/N) within 2MASS) and that the data base flag parametrizing source contamination and confusion (cc_flg) was 000, which together indicate a quality detection with signal-to-noise ratio >10 (e.g. Pokorny 2004). Our cross-matching returned a total of 381 objects from our *R*-band limited sample. These were visually inspected to identify any 2MASS counterparts that were clearly associated with different optical sources, as well as some very low signal-to-noise optical counterparts that appeared to be noise. Of the 381 cross-matched objects, 258 passed the visual inspection. The same colour, magnitude and quality constraints were applied to the SIPS catalogue objects, adding an additional 559 objects to our

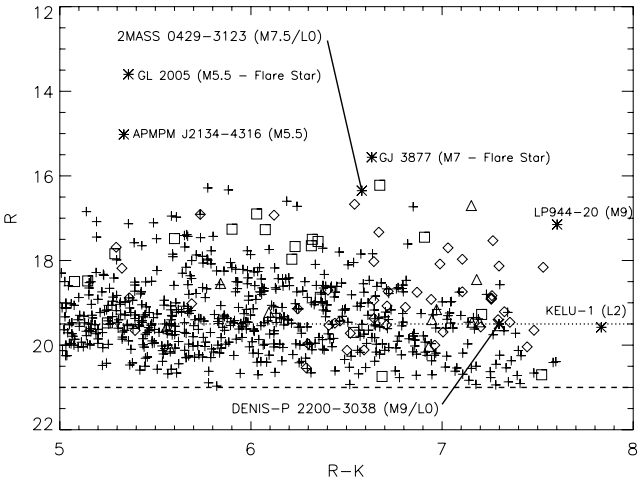

Figure 1. R versus $R - K$ colour-magnitude diagram for the new high proper motion red object catalogue. Catalogue objects are plotted as small crosses. Several previously studied interesting objects within the survey volume are highlighted as asterisks. We plot objects with known spectral types M5–M6.5, M7–M8.5 and M9+ as squares, diamonds and triangles, respectively. The dashed and dotted lines show the R-band magnitude limits for the new catalogue and the LEHPM, respectively.

red catalogue. There are thus 817 objects in our final high proper motion red object catalogue.

Fig. 1 shows an R versus $R - K_s$ colour magnitude diagram for our catalogue. We overplot the R-band limit of this new catalogue (dashed line), as well as that of the LEHPM (dotted line) for comparison.

2.3 Cross-matching with DENIS

Although the Deep Near Infrared Survey of the Southern Sky (DENIS) does not cover as much sky, it offers I-band photometry that is more accurate than SuperCOSMOS. Accuracies of <0.1 mag are typical of DENIS I-band photometry (Epchtein et al. 1997), SuperCOSMOS has absolute photometric uncertainties of ∼0.3 mag. We thus cross-matched our red object catalogues with the DENIS data base using the VizieR interface tool at Centre de Données Astronomiques de Strasbourg (CDS), selecting objects within a search radius of 10 arcsec (to allow for high proper motion) and a DENIS J-band magnitude within 0.3 mag of the 2MASS detection to minimize spurious matches. In total, 482 red object catalogue sources had a DENIS counterpart (out of a total of 817) in our cross-match, and we use this DENIS photometry in preference to the SuperCOSMOS I-band measurements where it is available.

3 SELECTING THE MOVING GROUP CANDIDATES

3.1 The moving groups

We chose to consider the five MGs assessed in Montes et al. (2001), namely the Pleiades, Castor, Hyades, Sirius (also known as Ursa Major) and IC2391 MGs. These are relatively well studied, with previous work producing lists of kinematic members (Eggen 1983a,b, 1991; Montes et al. 2001; López-Santiago et al. 2006).

Table 1 summarizes the physical and astrometric properties of these MGs. Properties are generally taken from Montes et al. (2001) which represents a recent and broad assessment of these groups. However, we have included updates where available, and also present metallicity estimates for the MGs. Space velocities UVW are given, where a positive U is towards the Galactic centre, a positive V is in the direction of Galactic rotation and a positive W is in the direction of the Galactic north pole. It should be noted that the Pleiades MG age has a significantly larger range than the other MGs. This is due to this MG actually being made up of a number of separate components with a range of ages (see Asiain, Figueras & Torra 2000; Makarov 2003; López-Santiago et al. 2006), although we treat the MG as a single component in this work.

Table 1. The five MGs and their properties.

MG	Age (Myr)	Metallicity [Fe/H]	U	V (km s^{-1})	W
Pleiades	20–150	-0.034 ± 0.024^a	−11.6	−21.0	−11.4
Hyades	600	0.13 ± 0.01^b	−39.7	−17.7	−2.4
Sirius	300	-0.09 ± 0.04^a	14.9	1.0	−10.7
IC2391	35–55	-0.03 ± 0.07^c	−20.6	−15.7	−9.1
Castor	320^d	0.00 ± 0.04^e	−10.7	−8.0	−9.7

Note. Properties are from Montes et al. (2001) unless specified.
[a]Boesgaard & Friel (1990), [b]Paulson, Sneden & Cochran (2003), [c]Randich et al. (2001), [d]Ribas (2003) and [e] Paulson & Yelda (2006).

3.2 Astrometric selection

Objects that share the same space motion must all move towards some convergent point (CP) on the sky (the vanishing point of the space motion vector). To easily identify such objects, one must convert the two usual proper motion vectors (orientated in the RA and Dec. directions) into a new coordinate system, with the CP (of the MG in question) at the pole. The two new proper motion vectors will thus represent the proper motion towards the CP ($\mu_{\rm tcp}$), and the proper motion perpendicular to this direction ($\mu_{\rm pcp}$). We used transformation equations based on the derivations of Reid (1992) to achieve this.

As an example, Fig. 2 shows the converted proper motions for our ultracool dwarf catalogue objects when considering the IC2391 MG.

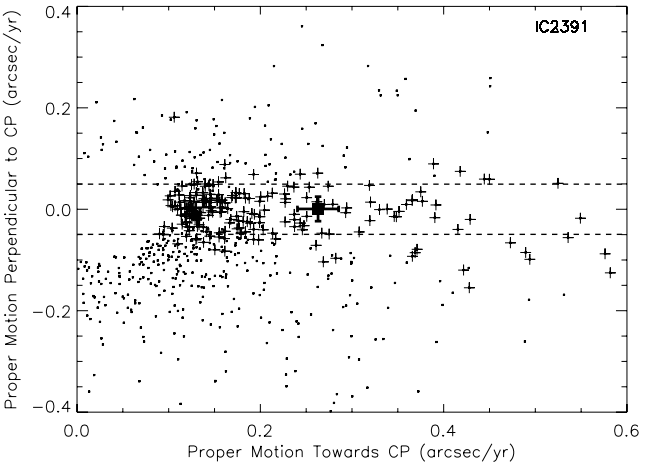

Figure 2. Plot showing the converted proper motion values $\mu_{\rm tcp}$ and $\mu_{\rm pcp}$ for our catalogue of objects, when considering the IC2391 MG. We have allowed for measurement uncertainty in the proper motions, and an intrinsic scatter of ±5 km s^{-1} in the space motion of the MG (see text). Objects that pass the astrometric selection criteria are highlighted as plus signs. Proper motion uncertainty and the expected intrinsic proper motion scatter are also indicated for DENIS-P J0021.0−4244 (filled square).

Simplistically, one would expect MG members to all have extremely small values of $\mu_{\rm pcp}$, with their motion being essentially towards the CP. However, there are several factors that will produce a scatter in $\mu_{\rm pcp}$ about zero. First, measurement uncertainty associated with the proper motions will contribute to a scatter. However, one also expects an intrinsic scatter in the space motions themselves, since a MG does not have an exact space motion. Both the (relatively slow) expansion velocity of the MG (a few kms^{-1}; Kroupa et al. 2001), and any gravitational influence of disc star interactions (disc heating) will contribute to an intrinsic scatter.

To take account of these effects, we allowed for a scatter of $\pm$5 km s^{-1}, which we converted into a proper motion velocity scatter using an astrometrically estimated distance. This distance was estimated assuming MG membership, when the total space motion of the group and the value of $\lambda_{\rm s}$ (angular distance between an object and the CP) for an object give the expected tangential velocity. Comparison of this velocity with the candidates total measured proper motion then yields an estimate of its distance assuming that the object is a MG member. This distance (d) is then,

$$d({\rm pc}) = \frac{V_{\rm S}\sin(\lambda_{\rm s})}{k\mu_{\rm tcp}}. \quad (1)$$

Here, $V_{\rm S}$ is the total space motion of the MG in question (in km s^{-1}) and $k = 4.74$, equivalent to 1 au yr^{-1} in units of km s^{-1}. An object was astrometrically selected as a possible MG member if its $\mu_{\rm pcp}$ was less than the estimated scatter or its 1σ proper motion uncertainties overlapped with this region (corresponding to $\pm$5 km s^{-1} at the astrometrically estimated distance). In the case of IC2391, such sources are highlighted in Fig. 2 as plus signs. As a specific example, Fig. 2 also shows the proper motion uncertainties and expected intrinsic proper motion scatter estimated for one example object, DENIS-P J0021.0-4244 (plotted as a solid square), a high proper motion object that we identify as a possible kinematic IC2391 MG member.

3.3 Photometric selection

By applying the astrometric test described in the previous section, we were able to identify catalogue objects whose proper motion was orientated towards the CPs of the MGs considered here (with some allowance made for both measurement uncertainty and intrinsic scatter in the astrometry). However, during this process, we also estimated a set of distances (see equation 1) for the objects based on the assumption that they are members of our MGs (which allowed us to assume their space motion, and compare this to their measured astrometry). We can use these estimated distances to plot objects on a series of colour-absolute magnitude diagrams (CMDs), and thus investigate if their location on these CMDs is consistent with expectations. Objects whose location on a CMD is not consistent can then be ruled out as possible members of that particular MG.

To assess if an object's CMD location is consistent, we defined a dwarf sequence on two CMDs using samples of canonical objects covering the full colour (and spectral type) range of our catalogue objects, but with distances from parallax measurements. For this purpose, we used M and L dwarf samples from Leggett (1992), Dahn et al. (2002), Knapp et al. (2004) and Vrba et al. (2004). Fig. 3 shows the M_J, $J-K$ CMD for this parallax sample, where M_J uncertainties result primarily from the parallax uncertainties. J- and K-band photometry is available for all our red catalogue objects, and this near-IR CMD could thus be used to photometrically test all astrometric candidates. I-band photometry was available for our catalogue objects, so we also used a selection criteria employing an M_J versus $I-J$ CMD (not shown here). Thus, objects were required to pass the photometric tests for both CMDs.

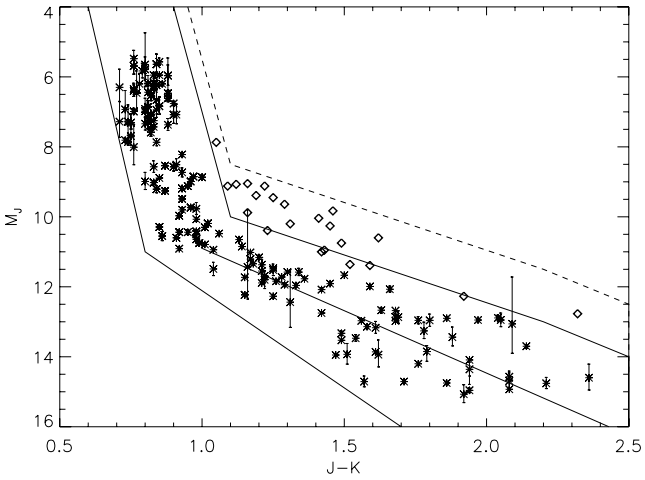

Figure 3. M_J versus $J-K$ CMD of known late M and early L dwarfs with measured parallax distances plotted as asterisks. A solid best-fitting line for these objects is overplotted. The region either side of this was defined as our ultracool dwarf sequence (bounded by solid lines). Note there are two alternative upper boundaries, one brighter by 1.5 mag to account for the potential youth of many of our selected objects (see text). For example, young Upper Scorpius members are plotted as diamonds.

In order to define CMD regions that represent the dwarf sequences in this range, we initially considered boundaries that fully (and conservatively) enclose the parallax sample, allowing for the inherent scatter. Much of this scatter presumably results from unresolved binarity and some spread in metallicity causing a scatter in both M_J and $J-K$ colour (e.g. fig. 7 of Leggett, Allard & Hauschildt 1998). However, an age spread is also a potential cause of scatter in this CMD, where some M_J values could be brighter due to younger objects not being fully contracted.

The parallax sample consists of bright field objects, with likely ages in the range $\sim$1–5 Gyr in general. We would therefore not expect significant scatter from a large number of young objects. However, all of our MGs are younger than this (e.g. IC2391 and the Pleiades MGs in particular). Theoretical isochrones (e.g. Baraffe et al. 1998) suggest that $\sim$20–50 Myr populations could be $\sim$1–1.5 mag brighter than more typical ($\sim$1–5 Gyr) field star samples, and we have therefore defined alternative upper boundaries in the two CMDs, to include any potentially brighter younger objects. This is also seen observationally; as an example we have plotted 21 BDs in the Upper Scorpius association (from Lodieu et al. 2008) as diamonds on Fig. 3. The association's age of 5 Myr is similar to the younger component of the Pleiades, so we would expect a similar shift in brightness. In our final candidate selections, we use the fainter upper boundaries when selecting Hyades MG candidates, and the brighter upper boundary when selecting candidate members of the other four MGs.

Fig. 4 shows an example of our photometric selection for the IC2391 MG. Catalogue objects are shown as small dots. Objects passing the astrometric selection are highlighted as plus signs, and those that also pass our photometric selection are shown as filled circles. Note that, in Fig. 4, a number of objects that pass the astrometric tests lie in the selection region of the CMD. Although these appear within the M_J versus $J-K$ selection region, they fail to be photometrically selected in the M_J versus $I-J$ CMD.

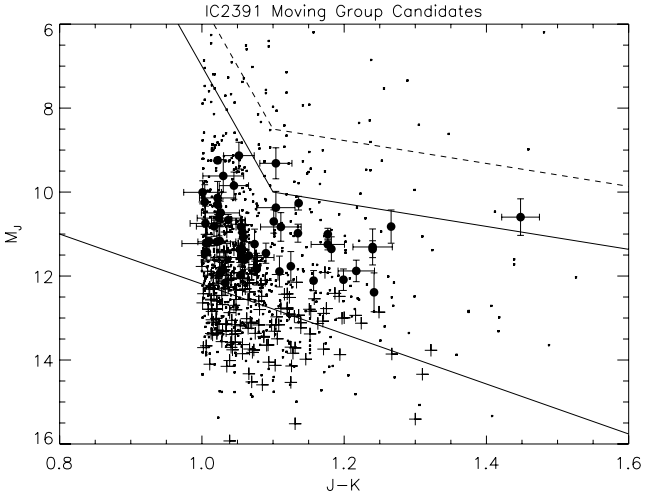

Figure 4. An example M_J, $J - K$ CMD selection for the IC2391 MG. The expected location of the dwarf sequence is enclosed by solid lines with the alternative upper boundary (for young sources) shown as a dashed line. Catalogue objects are shown as points. Objects passing the astrometric selection (see Section 3.2) are shown as plus signs. Objects also passing our photometric selection are shown as filled circles.

3.4 The moving group candidates

By considering each MG in turn we have identified 132 objects that are candidate members of one or more of the five MGs from Table 1; 47, 89, 11, 54 and 32 objects have candidature of the Pleiades, Hyades, Sirius, IC2391 and Castor MGs, respectively. Table 2 lists the candidates and gives their properties. The table also contains distance constraints for the candidates. Parallax distances are given where available. However, in the majority of cases parallaxes were not available so photometric distances ($d_{\rm phot}$) were estimated using an M_J–$(J - K)$ relation from our best-fitting line on the M_J versus $J - K$ CMD (Fig. 3) with some allowance for age uncertainty (i.e. possible membership or not of one or more MGs). We describe this method further in Section 4.3 where the same method has been used to provide distance estimates for the complete sample.

We can make an approximate estimate of the number of our MG candidates that we expect to be genuine, based on our knowledge from previous kinematic studies of the local disc population, and some assumptions about disc-age spread and structure. For a uniform disc age distribution from 0–10 Gyr, we would expect 6 per cent of disc objects to have ages <600 Myr. However, if stellar/substellar birth rate is constant (e.g. Reid et al. 1999; Burgasser 2004), some bias towards younger objects would be expected due to an increased disc scaleheight (H_z) for older populations. The exact form of this H_z variation is not well constrained, but $H_z(t)$ could change by up to a factor of ∼5 (Rocha-Pinto et al. 2000; Just 2003; Deacon & Hambly 2006; Pinfield et al. 2006) across the full disc age range. This would result in a factor ∼3 increase in the relative number of <600 Myr objects. Therefore, we may expect up to ∼18 per cent of our red object catalogue to have ages in this range, some ∼150 objects. While not all these young objects will be in MGs, kinematic studies based on *Hipparcos* (Dehnan 1998) indicate that approximately 50 per cent of such young objects would be expected to reside in kinematic groups, and therefore we may expect ∼75 objects from our red object catalogue to be genuine MG members.

4 CANDIDATE FOLLOW-UP

4.1 High-resolution spectroscopy

We observed seven objects using the Fibre-fed Extended Range Echelle Spectrograph (FEROS) echelle spectrometer mounted on the 2.2-m telescope based at La Silla (Chile) on the nights of 2006 December 29–30 from programme 078.C-0333(A) and 2007 June 16–17 from programme 079.C-0255(A). FEROS covers the wavelength 3500–9200 Å over 39 orders with a resolving power of 48 000 (Kaufer et al. 1997). It is equipped with a double filter system allowing the object and the sky to be simultaneously measured. We used exposure times that provided us with spectra of S/N ∼ 15–20 in the redder orders. In both observing runs, we experienced thin cloud and some time was lost to bad weather. Seeing was generally 1–1.3 arcsec.

Starlink software was used for bias subtraction, flat-field division and optimal extraction of the spectra. Bias subtraction was performed using the DEBIAS routine and the mean of the bias frames taken as part of the standard calibration for FEROS. The FIGARO routine BCLEAN allowed us to remove any cosmic ray contamination whilst sacrificing a minimal amount of signal. Lamp illuminated flat-fields were used to normalize the response of the detector. The routine ECHOMOP was used to trace and clip the orders, model the flat-field balance and sky background, and to extract the spectra. Finally, extracted spectra were wavelength calibrated using the Th-Ar illuminated images obtained after each observation.

4.2 Spectral types

To obtain spectral types, we used a variety of different spectral indices. Our spectra often had a low S/N at certain wavelengths, so indices were chosen for regions with good signal. The VO index from Kirkpatrick, Henry & Simons (1995), CaH from Kirkpatrick, Henry & McCarthy (1991), VO-a and TiO5 from Cruz & Reid (2002) and PC3, TiO1+TiO2 and VO1+VO2 from Martín et al. (1999) were calculated, giving a number of spectral types from which we took the mean to give an adopted spectral type. It should be noted that the TiO1+TiO2 and VO1+VO2 indices can infer two different spectral types and were thus only considered after we calculated the spectral type using other indices. The PC3 ratio covered low-signal regions of spectra, so it was not used. Table 3 shows the indices and spectral types for our FEROS objects with spectroscopic distances calculated using a spectral type-absolute J-magnitude relation from Cruz et al. (2003).

4.3 Space motions

To obtain radial velocities, we cross-correlated each individual order of the reduced spectra using an IDL routine that determines the digital cross-correlation of two arrays and finds the maximum cross-correlation function by fitting a Gaussian to the central peak. This provided a set of radial velocities for each object from the different echelle orders with usable S/N (5–7 orders per object). Our final radial velocities and associated uncertainties came from the mean and standard deviation of these measurements. A heliocentric correction was made to the measured shift between the object and the reference star so that the we could calculate radial velocities with respect to the Sun.

To allow for younger objects appearing intrinsically brighter, we created isochrones corresponding to the ages of our MGs and that of a field dwarf using atmospheric models from Baraffe et al. (1998). Approximating difference in absolute J-magnitude due to youth

Table 2. Properties of the 132 MG candidates.

Name	J-mag	$J-H$	$J-K_s$	$I-J^a$	R^a	PM_{RA} (mas yr^{-1})	$PM_{Dec.}$ (mas yr^{-1})	Total σ_{PM} (mas yr^{-1})	Distance (pc)^b	Sp. T	MG^c candidature
SIPS 0004−5721	14.01 ± 0.03	0.67 ± 0.04	1.07 ± 0.04	2.81 ± 0.30	19.78	157.0	−15.0	28.2	33–53	M7.0	CA, HY, IC, PL
SIPS 0007−2458	13.11 ± 0.02	0.67 ± 0.03	1.05 ± 0.03	2.66 ± 0.07	18.78	192.0	−59.0	13.6	23–36	M7.0^g	CA, IC, PL
2MASS J00202315−2346053	12.35 ± 0.02	0.63 ± 0.13	1.01 ± 0.03	2.31 ± 0.05	17.71	340.2	−65.0	20.2	17–27	M6.0^g	IC
DENIS-P J0021.0−4244	13.52 ± 0.03	0.71 ± 0.04	1.22 ± 0.04	3.27 ± 0.11	19.46	262.4	−17.3	33.0	21–34	≥M9.0^g	CA, HY, IC
SIPS 0027−5401	12.36 ± 0.02	0.65 ± 0.04	1.02 ± 0.03	2.46 ± 0.09	17.80	429.0	−18.0	33.0	17–27	M7.0	HY, IC
SIPS 0030−6719	14.32 ± 0.03	0.74 ± 0.05	1.20 ± 0.04	2.99 ± 0.16	–	200.0	2.0	25.0	32–50	M7.5	HY, IC, PL
SIPS 0031−3807	14.64 ± 0.03	0.68 ± 0.05	1.05 ± 0.05	2.20 ± 0.10	19.17	117.0	−32.0	19.6	47–74	M6.0	IC, PL
SIPS 0039−2256	14.30 ± 0.03	0.67 ± 0.04	1.02 ± 0.05	2.41 ± 0.30	20.24	224.0	44.0	25.5	42–66	M7.0	HY
DENIS-P J004135.3−562112	11.96 ± 0.02	0.64 ± 0.03	1.10 ± 0.03	2.48 ± 0.05	17.97	92.0	−62.1	21.0	12–20	M7.5^g	CA, PL, SI
SIPS 0054−4142	12.62 ± 0.03	0.67 ± 0.04	1.00 ± 0.04	1.92 ± 0.05	17.11	64.0	−108.0	17.5	20–31	M5.0	CA
SIPS 0058−0651	14.31 ± 0.03	0.87 ± 0.04	1.41 ± 0.04	3.36 ± 0.05	–	229.0	−200.0	36.9	23–36	L0^g	PL
2MASS J01023244−2915370	15.63 ± 0.06	0.66 ± 0.07	1.05 ± 0.10	2.14 ± 0.18	20.16	131.5	27.6	32.1	74–118	M6.0	HY
2MASS J01025334−3056300	14.70 ± 0.04	0.62 ± 0.06	1.06 ± 0.06	2.30 ± 0.12	19.38	126.2	−1.6	21.6	47–75	M6.5	HY, IC
SIPS 0105−1826	13.26 ± 0.02	0.68 ± 0.04	1.01 ± 0.03	1.92 ± 0.06	17.45	239.0	42.0	11.2	26–42	M5.0	HY
SIPS 0109−5100	12.23 ± 0.02	0.69 ± 0.03	1.14 ± 0.03	3.04 ± 0.05	18.08	207.0	87.0	17.5	13–21	M8.5^g	CA, HY, IC
NLTT 3868	11.69 ± 0.02	0.76 ± 0.03	1.27 ± 0.03	3.07 ± 0.30	–	375.0	22.0	75.1	$9.6^{+0.2}_{-0.2}$ $^{(d)}$	M9.0^g	CA, HY, IC
LEHPM 1289	13.60 ± 0.03	0.65 ± 0.10	1.01 ± 0.03	2.40 ± 0.30	18.66	366.3	−4.4	35.4	31–49	M7.0	HY
SIPS 0115−2715	14.52 ± 0.04	0.55 ± 0.04	1.00 ± 0.06	2.30 ± 0.31	18.74	149.0	32.0	12.2	48–76	M6.5	HY
2MASS J01230050−3610306	13.64 ± 0.02	0.53 ± 0.06	1.45 ± 0.03	1.76 ± 0.08	17.58	124.5	57.4	30.5	15–25	M4.5	HY, IC
SIPS 0126−1946	14.26 ± 0.03	0.65 ± 0.05	1.02 ± 0.05	2.01 ± 0.30	19.34	210.0	−11.0	47.0	41–66	M5.5	HY
LEHPM 1563	12.66 ± 0.03	0.62 ± 0.05	1.00 ± 0.03	3.13 ± 0.30	18.47	290.3	131.5	21.4	20–32	M8.5	HY
SIPS 0141−4232	14.67 ± 0.04	0.68 ± 0.05	1.06 ± 0.05	2.35 ± 0.14	–	108.0	19.0	20.4	47–74	M6.5	HY, IC, PL
SIPS 0152−4003	15.26 ± 0.05	0.77 ± 0.06	1.14 ± 0.09	2.55 ± 0.19	–	192.0	26.0	26.3	54–86	M7.0	HY
2MASS J01531169−5122242	13.45 ± 0.03	0.57 ± 0.05	1.03 ± 0.04	2.27 ± 0.08	18.41	123.2	41.0	21.4	28–44	M6.5	HY, IC, PL
2MASS J02041803−3945064	13.39 ± 0.03	0.68 ± 0.04	1.10 ± 0.04	2.51 ± 0.13	18.81	119.1	16.6	23.5	24–38	M7.0	CA, HY, IC, PL
SIPS 0207−3721	12.44 ± 0.03	0.61 ± 0.04	1.06 ± 0.04	2.63 ± 0.06	18.02	429.0	148.0	14.9	$23.9^{+8.4}_{-5.0}$ $^{(e)}$	M7.0^g	HY
SIPS 0212−6049	13.31 ± 0.03	0.73 ± 0.04	1.15 ± 0.04	2.44 ± 0.09	18.61	112.0	−25.0	12.4	21–34	M7.0	SI
SIPS 0214−3237	14.01 ± 0.03	0.67 ± 0.04	1.06 ± 0.04	2.22 ± 0.30	–	148.0	42.0	34.2	34–54	M6.0	HY, IC
2MASS J02155647−3456036	14.56 ± 0.03	0.68 ± 0.04	1.07 ± 0.05	1.82 ± 0.09	18.65	160.9	55.9	34.6	44–70	M5.0	HY
SIPS 0219−7137	13.59 ± 0.03	0.66 ± 0.04	1.08 ± 0.04	2.15 ± 0.09	18.64	173.0	109.0	21.1	27–44	M6.0	HY
SIPS 0223−4424	14.75 ± 0.04	0.70 ± 0.06	1.02 ± 0.05	2.13 ± 0.30	19.32	156.0	80.0	15.7	51–82	M6.0	HY
2MASS J02262591−1839437	14.56 ± 0.03	0.70 ± 0.06	1.12 ± 0.06	2.38 ± 0.31	20.23	193.2	67.0	36.6	40–64	M6.5	HY
SIPS 0235−0711	12.45 ± 0.03	0.63 ± 0.04	1.02 ± 0.04	2.01 ± 0.06	–	286.0	75.0	18.7	18–28	M5.5^g	HY
SIPS 0236−1616	14.43 ± 0.03	0.69 ± 0.05	1.11 ± 0.04	2.66 ± 0.13	–	130.0	−24.0	24.3	39–61	M7.5	IC, PL, SI
SIPS 0239−1735	14.29 ± 0.03	0.77 ± 0.05	1.25 ± 0.05	3.31 ± 0.16	–	88.0	−110.0	32.0	29–46	L0^g	CA, PL, SI
2MASS J02495798−2147267	13.27 ± 0.03	0.60 ± 0.03	1.02 ± 0.04	2.18 ± 0.30	18.59	150.9	31.2	37.4	26–41	M6.0	HY, IC
SIPS 0250−3056	15.47 ± 0.07	0.69 ± 0.11	1.14 ± 0.11	2.20 ± 0.32	20.03	127.0	18.0	29.3	60–95	M6.0	HY
SIPS 0255−7711	14.96 ± 0.04	0.68 ± 0.07	1.05 ± 0.08	1.90 ± 0.14	19.50	87.0	101.0	29.1	55–87	M5.0	HY
SIPS 0313−1347	14.41 ± 0.02	0.71 ± 0.03	1.08 ± 0.05	1.83 ± 0.10	18.73	100.0	14.0	15.1	40–64	M5.0	HY
SIPS 0317−6415	14.81 ± 0.04	0.64 ± 0.06	1.03 ± 0.05	1.86 ± 0.09	18.88	69.0	89.0	16.4	52–83	M5.0	HY
SIPS 0324−0050	14.77 ± 0.04	0.61 ± 0.06	1.03 ± 0.07	2.52 ± 0.31	–	107.0	−37.0	19.9	51–81	M7.0	SI
SIPS 0329−5747	13.98 ± 0.03	0.61 ± 0.04	1.03 ± 0.04	2.76 ± 0.30	19.46	140.0	109.0	19.2	36–57	M7.5	HY, IC

Table 2 – *continued*

Name	J-mag	$J-H$	$J-K_s$	$I-J^a$	R^a	PM_{RA} (mas yr^{-1})	$PM_{Dec.}$ (mas yr^{-1})	Total σ_{PM} (mas yr^{-1})	Distance (pc)^b	Sp. T^c	MG^d candidature
2MASS J03341065−2130343	11.91 ± 0.02	0.61 ± 0.04	1.05 ± 0.03	1.92 ± 0.30	16.90	123.6	7.2	20.0	13–21	M6.0[g]	IC
SIPS 0336−1437	15.41 ± 0.03	0.65 ± 0.06	1.05 ± 0.08	2.49 ± 0.31	–	111.0	49.0	25.1	66–105	M7.0	HY
LP 944−20	10.73 ± 0.02	0.71 ± 0.04	1.18 ± 0.03	3.43 ± 0.04	17.15	355.0	273.8	27.5	5.0 ± 0.1[(g)]	M9.0[(f)]	CA, IC
SIPS 0401−4253	13.57 ± 0.03	0.67 ± 0.03	1.07 ± 0.04	2.47 ± 0.10	18.74	76.0	−71.0	17.7	27–44	M7.0	SI
2MASS J04075679−5535544	13.23 ± 0.03	0.64 ± 0.04	1.02 ± 0.04	2.07 ± 0.07	17.99	38.2	143.4	17.2	25–41	M5.5	IC
SIPS 0424−6243	14.02 ± 0.03	0.65 ± 0.04	1.01 ± 0.05	2.06 ± 0.09	18.49	10.0	123.0	20.1	37–60	M5.5	IC
2MASS J04291842−3123568	10.87 ± 0.02	0.66 ± 0.03	1.10 ± 0.03	2.44 ± 0.04	16.35	106.1	69.3	23.6	7–12	M7.0/L1[g]	CA, IC
SIPS 0436−3429	14.73 ± 0.03	0.62 ± 0.06	1.01 ± 0.06	2.41 ± 0.14	20.09	81.0	92.0	29.1	52–82	M7.0	HY
SIPS 0441−6413	14.76 ± 0.03	0.69 ± 0.05	1.04 ± 0.05	2.25 ± 0.12	19.04	13.0	114.0	25.2	50–80	M6.5	IC
2MASS J04454336−5321345	12.85 ± 0.02	0.60 ± 0.06	1.00 ± 0.03	2.73 ± 0.07	18.47	343.8	485.8	12.9	22–35	M7.5	HY
SIPS 0501−7705	14.09 ± 0.03	0.61 ± 0.05	1.08 ± 0.05	2.84 ± 0.11	20.37	67.0	91.0	17.2	34–55	M7.0	PL
2MASS J05023867−3227500	12.44 ± 0.03	0.63 ± 0.19	1.00 ± 0.04	2.11 ± 0.30	17.67	62.6	−171.9	20.8	18–29	M6.5[g]	SI
2MASS J05280562−5919471	14.56 ± 0.04	0.53 ± 0.21	1.02 ± 0.06	2.09 ± 0.11	19.49	77.1	152.7	29.4	47–75	M5.5	HY
2MASS J05390417−4708060	13.26 ± 0.03	0.65 ± 0.04	1.04 ± 0.04	2.56 ± 0.07	18.59	30.8	350.0	16.5	25–40	M7.0	HY
2MASS J06003375−3314268	13.20 ± 0.03	0.78 ± 0.18	1.19 ± 0.04	2.23 ± 0.10	18.73	−28.3	153.7	29.3	19–30	M7.5[g]	HY
2MASS J06361472−3241315	13.33 ± 0.02	0.61 ± 0.03	1.04 ± 0.03	2.71 ± 0.06	18.43	−20.3	97.9	23.1	26–41	M7.5	HY
SIPS 0648−6537	13.06 ± 0.03	0.63 ± 0.04	1.00 ± 0.04	2.50 ± 0.09	18.53	9.0	−199.0	14.0	24–38	M7.0	SI
SIPS 0650−5003	14.34 ± 0.03	0.66 ± 0.04	1.01 ± 0.05	2.52 ± 0.10	19.73	4.0	228.0	17.0	43–69	M7.0	HY
SIPS 0745−5554	15.44 ± 0.06	0.54 ± 0.10	1.10 ± 0.10	2.32 ± 0.16	20.66	14.0	125.0	29.2	63–100	M6.5	HY
SIPS 0752−6621	15.16 ± 0.05	0.73 ± 0.07	1.04 ± 0.08	2.56 ± 0.21	20.39	8.0	114.0	26.1	61–96	M7.0	HY
SIPS 0913−0426	14.65 ± 0.05	0.72 ± 0.07	1.08 ± 0.07	2.85 ± 0.14	–	131.0	22.0	25.3	45–71	M7.0	CA, HY, IC
SIPS 1039−4110	11.97 ± 0.02	0.65 ± 0.03	1.02 ± 0.03	2.35 ± 0.30	–	25.0	−173.0	8.1	14–22	M6.0[g]	SI
SIPS 1124−2019	13.44 ± 0.03	0.62 ± 0.04	1.00 ± 0.04	2.72 ± 0.07	19.17	129.0	−19.0	27.3	29–46	M7.0	CA, IC
SIPS 1228−1547	14.38 ± 0.03	1.03 ± 0.04	1.61 ± 0.04	3.51 ± 0.20	–	250.0	−331.0	64.2	17–27	L1	PL
DENIS-P J125052.6−212113	11.16 ± 0.02	0.61 ± 0.04	1.03 ± 0.03	2.62 ± 0.04	16.67	456.5	−319.9	24.1	9–15	M7.5[g]	PL
SIPS 1314−3212	13.76 ± 0.03	0.62 ± 0.04	1.01 ± 0.04	2.84 ± 0.30	19.54	142.0	−160.0	28.3	33–53	M7.0	PL
SIPS 1329−4147	13.65 ± 0.02	0.85 ± 0.04	1.38 ± 0.03	3.30 ± 0.09	19.30	293.0	−302.0	33.9	17–28	M9.0[g]	PL
SIPS 1408−0435	15.00 ± 0.04	0.81 ± 0.06	1.17 ± 0.07	2.34 ± 0.20	–	50.0	−97.0	23.7	45–72	M6.5	PL
SIPS 1450−1353	14.47 ± 0.03	0.65 ± 0.06	1.02 ± 0.06	2.74 ± 0.13	19.86	52.0	−118.0	14.3	45–72	M7.5	PL
2MASS J15072779−2000431	11.71 ± 0.02	0.67 ± 0.09	1.05 ± 0.03	2.72 ± 0.07	17.33	114.2	−76.7	21.8	12–19	M7.5[g]	CA, IC, PL, SI
SIPS 1632−0631	12.74 ± 0.02	0.70 ± 0.03	1.12 ± 0.03	2.86 ± 0.05	–	29.0	−366.0	37.1	17–27	M7.0[g]	PL
SIPS 1758−6811	13.99 ± 0.03	0.63 ± 0.04	1.00 ± 0.05	2.03 ± 0.08	18.59	3.0	−182.0	14.0	37–59	M5.5	HY
SIPS 1826−6542	10.57 ± 0.03	0.61 ± 0.03	1.02 ± 0.03	2.34 ± 0.30	16.22	6.0	−311.0	9.0	7–11	M6.5	CA, HY, IC, PL
SIPS 1903−3150	13.16 ± 9.00	0.70 ± 12.73	1.03 ± 0.04	1.68 ± 0.06	–	91.0	−128.0	33.0	24–38	M4.5	PL
SIPS 1930−1943	12.34 ± 0.03	0.65 ± 0.04	1.07 ± 0.04	2.48 ± 0.05	17.85	242.0	−89.0	26.6	15–25	M6.5[g]	HY
SIPS 1949−7136	13.92 ± 0.03	0.80 ± 0.04	1.18 ± 0.04	2.69 ± 0.09	18.43	36.0	−183.0	26.5	27–43	M7.5	HY, IC, PL
SIPS 1955−4137	14.86 ± 0.04	0.75 ± 0.05	1.12 ± 0.06	3.09 ± 0.21	20.38	73.0	−98.0	21.4	46–73	M8.0	CA, HY, IC, PL
SIPS 2000−7523	12.73 ± 0.03	0.77 ± 0.04	1.22 ± 0.04	2.95 ± 0.07	18.05	179.0	−85.0	25.5	14–23	M9.0[g]	CA
2MASS J20012463−5949000	13.24 ± 0.02	0.64 ± 0.03	1.03 ± 0.04	2.26 ± 0.06	18.61	163.3	−54.4	28.1	25–40	M6.5	CA
SIPS 2014−2016	12.54 ± 0.02	0.69 ± 0.03	1.09 ± 0.04	2.78 ± 0.30	–	248.0	−112.0	31.8	16–26	M7.5[g]	CA, HY, IC

Table 2 – *continued*

Name	J-mag	$J-H$	$J-K_s$	$I-J$[a]	R[a]	PM_{RA} (mas yr^{-1})	$PM_{Dec.}$ (mas yr^{-1})	Total σ_{PM} (mas yr^{-1})	Distance (pc)[b]	Sp. T[c]	MG[d] candidature
2MASS J20312749−5041134	13.34 ± 0.03	0.65 ± 0.09	1.03 ± 0.03	2.00 ± 0.08	18.06	161.4	−160.3	37.4	26–42	M5.5	HY
SIPS 2036−2537	14.21 ± 0.03	0.62 ± 0.05	1.07 ± 0.05	2.56 ± 0.09	19.91	131.0	−134.0	15.6	37–59	M7.0	PL
SIPS 2039−1126	13.79 ± 0.03	0.66 ± 0.05	1.11 ± 0.04	2.66 ± 0.08	19.17	64.0	−105.0	15.3	28–45	M8.0[g]	CA, PL
SIPS 2041−1006	14.93 ± 0.04	0.67 ± 0.05	1.08 ± 0.05	2.33 ± 0.11	–	57.0	−96.0	23.3	51–81	M6.5	PL
SIPS 2045−6332	12.62 ± 0.03	0.81 ± 0.04	1.41 ± 0.04	3.33 ± 0.10	19.03	97.0	−201.0	18.8	10–16	M9.5	CA, PL
SIPS 2049−1716	11.81 ± 0.03	0.60 ± 0.04	1.01 ± 0.03	2.19 ± 0.30	16.93	369.0	−142.0	44.0	13–21	M7.0[g]	HY, IC
SIPS 2049−1944	12.85 ± 0.02	0.63 ± 0.03	1.07 ± 0.03	2.59 ± 0.05	18.58	179.0	−279.0	13.0	20–31	M7.5[g]	PL
SIPS 2049−3130	12.65 ± 0.02	0.66 ± 0.03	1.06 ± 0.03	2.69 ± 0.06	18.10	168.0	−184.0	38.9	18–29	M7.5	CA, IC, PL
SIPS 2057−1407	14.71 ± 0.03	0.67 ± 0.05	1.05 ± 0.05	2.80 ± 0.17	–	179.0	12.0	30.1	48–77	M7.5	HY
SIPS 2100−6255	14.73 ± 0.03	0.70 ± 0.04	1.05 ± 0.05	1.81 ± 0.13	–	65.0	−110.0	19.7	49–78	M5.0	HY
SIPS 2105−1305	15.29 ± 0.05	0.71 ± 0.08	1.24 ± 0.08	2.56 ± 0.31	–	114.0	−50.0	29.5	47–74	M7.0	HY, IC
2MASS J21062089−4044519	13.28 ± 0.02	0.62 ± 0.09	1.01 ± 0.03	2.21 ± 0.30	18.65	150.2	−83.1	35.9	27–42	M6.0	HY, IC
SIPS 2114−4339	13.02 ± 0.02	0.66 ± 0.03	1.06 ± 0.03	2.55 ± 0.09	18.61	49.0	−148.0	18.0	21–34	M7.0	CA
SIPS 2118−1441	14.65 ± 0.04	0.63 ± 0.06	1.03 ± 0.06	2.24 ± 0.11	19.05	114.0	−66.0	17.5	48–77	M6.0	PL
SIPS 2119−0740	14.07 ± 0.03	0.65 ± 0.05	1.05 ± 0.04	2.55 ± 0.09	–	152.0	−117.0	19.2	35–57	M7.0	IC, PL
HB 2124−4228	13.32 ± 0.02	0.66 ± 0.03	1.14 ± 0.03	2.76 ± 0.09	19.35	97.2	−170.4	49.2	35.7 ± 10.1[f]	M8.5[g]	PL
SIPS 2128−3254	11.56 ± 0.03	0.65 ± 0.05	1.05 ± 0.05	1.82 ± 0.30	16.28	338.0	−166.0	21.0	11–18	M5.0	HY
SIPS 2132−6248	14.45 ± 0.03	0.69 ± 0.05	1.02 ± 0.05	2.30 ± 0.12	19.08	100.0	−12.0	24.2	45–71	M6.5	CA
SIPS 2144−7518	14.53 ± 0.04	0.62 ± 0.05	1.01 ± 0.06	2.23 ± 0.13	20.11	102.0	−124.0	19.8	47–75	M6.0	HY
SIPS 2151−4017	11.45 ± 0.02	0.69 ± 0.03	1.03 ± 0.03	2.04 ± 0.04	16.60	471.0	−283.0	32.8	11–17	M5.5	HY
DENIS-P J220002.0−30383	13.44 ± 0.03	0.79 ± 0.05	1.24 ± 0.04	2.76 ± 0.30	19.50	198.7	−66.4	45.8	20–31	M9.0/L0[g]	CA, HY, IC
SIPS 2200−2756	13.73 ± 0.03	0.66 ± 0.04	1.03 ± 0.04	2.24 ± 0.30	18.54	156.0	−8.0	16.0	31–50	M6.0	HY
2MASS J22071031−6917142	13.71 ± 0.03	0.66 ± 0.05	1.02 ± 0.04	2.55 ± 0.14	19.00	130.8	−50.7	29.9	31–50	M7.0	CA, HY, IC, PL
LEHPM 4480	13.56 ± 0.03	0.61 ± 0.04	1.06 ± 0.04	2.19 ± 0.09	18.16	259.8	−135.8	17.0	28–44	M6.0	HY
SIPS 2219−3944	15.38 ± 0.05	0.70 ± 0.07	1.03 ± 0.08	2.01 ± 0.16	19.47	106.0	−57.0	23.7	67–107	M5.5	HY
2MASS J22220368−4919234	14.55 ± 0.03	0.60 ± 0.05	1.01 ± 0.05	2.10 ± 0.30	19.66	66.8	−122.4	32.5	48–76	M6.0	PL
SIPS 2227−4238	14.60 ± 0.03	0.69 ± 0.05	1.02 ± 0.06	2.14 ± 0.13	19.22	103.0	−59.0	22.0	48–76	M6.0	HY, IC, PL
2MASS J22310865−4443184	13.00 ± 0.02	0.64 ± 0.05	1.02 ± 0.03	2.07 ± 0.30	17.77	163.2	−9.5	32.4	23–36	M5.5	CA, HY, IC
LEHPM 4908	12.68 ± 0.02	0.60 ± 0.03	1.04 ± 0.03	2.36 ± 0.06	17.74	219.7	−63.1	14.4	19–30	M6.5	HY, IC
2MASS J22424129−2659272	13.35 ± 0.03	0.66 ± 0.08	1.03 ± 0.04	2.17 ± 0.09	17.91	99.3	−26.1	20.1	26–42	M6.0	CA, HY, IC
2MASS J22485685−6224060	14.91 ± 0.05	0.72 ± 0.05	1.06 ± 0.08	2.00 ± 0.31	19.97	128.7	−102.2	40.3	52–83	M5.5	HY
2MASS J22545811−3228522	13.58 ± 0.03	0.63 ± 0.04	1.01 ± 0.04	2.01 ± 0.30	18.55	55.4	−83.9	23.4	30–48	M5.5	CA, PL
SIPS 2302−3939	15.39 ± 0.05	0.69 ± 0.09	1.09 ± 0.08	2.07 ± 0.16	19.98	118.0	−49.0	22.8	62–99	M5.5	HY
SIPS 2307−3910	15.08 ± 0.05	0.78 ± 0.06	1.25 ± 0.06	2.75 ± 0.19	–	215.0	−6.0	21.0	42–66	M7.5	HY
2MASS J23113033−5256301	14.18 ± 0.03	0.62 ± 0.05	1.01 ± 0.05	2.30 ± 0.30	19.11	141.4	−43.8	29.3	40–64	M6.5	HY, IC, PL
SIPS 2318−4919	13.76 ± 0.03	0.69 ± 0.04	1.07 ± 0.04	2.30 ± 0.30	19.29	227.0	−25.0	22.1	30–47	M8.0[g]	HY
2MASS J23214341−6106353	13.39 ± 0.02	0.63 ± 0.10	1.00 ± 0.04	1.71 ± 0.07	18.25	110.7	−58.7	16.9	28–45	M4.5	IC, PL
SIPS 2322−6357	14.26 ± 0.03	0.61 ± 0.04	1.06 ± 0.05	2.19 ± 0.13	19.39	122.0	−28.0	18.4	39–61	M7.5[g]	HY, IC, PL
SIPS 2326−3708	14.97 ± 0.05	0.68 ± 0.07	1.03 ± 0.08	2.66 ± 0.31	–	158.0	−19.0	23.2	56–89	M7.5	HY, IC
SIPS 2339−5038	15.52 ± 0.08	0.68 ± 0.10	1.05 ± 0.11	2.06 ± 0.19	20.12	137.0	16.0	27.2	70–112	M5.5	HY
SIPS 2341−3550	13.53 ± 0.03	0.55 ± 0.04	1.10 ± 0.04	2.55 ± 0.08	18.86	154.0	−28.0	21.4	26–41	M7.0	CA, HY, IC
SIPS 2343−2947	13.59 ± 0.02	0.64 ± 0.03	1.08 ± 0.04	2.76 ± 0.30	19.09	257.0	−8.0	22.0	27–44	M7.5	HY, IC

Table 2 – *continued*

Name	J-mag	$J-H$	$J-K_s$	$I-J^a$	R^a	PM_{RA} (mas yr^{-1})	$PM_{Dec.}$ (mas yr^{-1})	Total σ_{PM} (mas yr^{-1})	Distance (pc)^b	Sp. T^c	MG^d candidature
2MASS J23445797−6809398	13.98 ± 0.03	0.62 ± 0.05	1.02 ± 0.04	2.50 ± 0.10	19.43	177.6	−83.8	30.6	36–58	M6.5^g	PL
SIPS 2347−1821	13.07 ± 0.03	0.60 ± 0.04	1.02 ± 0.04	2.23 ± 0.30	18.18	219.0	41.0	17.3	23–38	M6.0	HY
SIPS 2348−3136	14.03 ± 0.03	0.73 ± 0.04	1.16 ± 0.04	2.80 ± 0.30	19.52	231.0	−54.0	27.7	30–47	M7.5	IC
SIPS 2350−6915	14.20 ± 0.03	0.71 ± 0.05	1.07 ± 0.05	2.49 ± 0.10	19.23	164.0	−11.0	26.1	37–59	M7.0	HY, IC, PL
2MASS J23524913−2249295	13.02 ± 0.02	0.70 ± 0.07	1.07 ± 0.04	2.64 ± 0.30	18.33	222.0	−175.0	32.5	21–34	M7.5	PL
SIPS 2353−4123	14.39 ± 0.03	0.65 ± 0.05	1.06 ± 0.05	2.39 ± 0.10	19.02	148.0	−1.0	23.0	41–65	M6.0^g	HY, IC
SIPS 2354−4210	15.30 ± 0.05	0.62 ± 0.07	1.07 ± 0.08	1.89 ± 0.31	19.48	111.0	−28.0	25.7	61–97	M5.0	HY
LEHPM 6542	13.32 ± 0.02	0.66 ± 0.15	1.11 ± 0.04	2.64 ± 0.30	18.41	184.9	−4.6	31.4	23–37	M7.5	CA, HY, IC

Note. *J*-, *H*- and *K*-band photometry is from 2MASS. *R*-band photometry is from SuperCOSMOS. *I*-band photometry is from DENIS where available, or from SuperCOSMOS. Distances are parallaxes where available, or are estimated using an M_J–$(J-K)$ relation from our best-fitting line on the M_J versus $J-K$ CMD with some additional allowance for age uncertainty (see Section 3.4). Spectral types are from the literature where available, or have been determined from M_J versus spectral type relations from Dahn et al. (2002) for $I-J \geq 2.8$ and Leggett (1992) for $I-J < 2.8$. The potential MG membership for each candidate is shown in the last column. CA = Castor, IC = IC2391, PL = Pleiades, HY = Hyades, SI = Sirius.

[a] *R*-band uncertainties ∼0.3 mag (Hambly, Irwin & MacGillivray 2001).

[b] Photometric distance from Section 3.4.

[c] Moving groups from Section 3.4.

[d] Costa et al. (2005), [e] Costa et al. (2006), [f] Tinney (1996), [g] SpT in literature – Refs: Tinney (1998), Kirkpatrick et al. (2000), Burgasser et al. (2002), Cruz & Reid (2002), Gizis (2002), Cruz et al. (2003), Lodieu et al. (2005), Siegler et al. (2005), Burgasser & McElwain (2006), Basri & Reiners (2006) and Phan-Bao & Bessel (2006).

(according to each object's candidate group membership from Table 2) was used in the Dahn distance–spectral type relation to give a new corrected distance assuming group membership; thus, providing a number of distances for each of the radial velocity objects. These distances (or any parallaxes available from the literature) were used in a case-by-case basis with proper motions and radial velocities to derive space motions for these objects using the transformation matrices of Johnson & Soderblom (1987).

To assess the potential MG membership of these objects, we compared their kinematics with the measured space motions of available samples of higher mass MG members from the literature (Barrado Y Navacués 1998; Montes et al. 2001). Figs 5 and 6 show the *UV* and *VW* space motions of these higher mass samples. We trace boxes around each set of MG members (in each diagram), so as to contain a high fraction (with the occasional exception of one or two outliers) of the members. In this way, we were able to effectively define the space motion ranges that are representative of each MG.

Table 4 shows the radial velocity objects with their properties according to potential group membership in Table 2. Where, after evaluation, an object appears to be a kinematic member, the values are highlighted in bold. Figs 7 and 8 show the space motions of the 10 radial velocity objects (seven FEROS objects and three from the literature). Kinematic members are plotted as symbols corresponding to their kinematic group membership, objects that are not kinematic members have all their possible space motions plotted as crosses. We are able to reject four objects as possible MG members using our kinematic constraints, and thus have six candidates that are kinematically consistent with MG membership. SIPS 2049−1716 and SIPS 2128−3254 are found to be kinematic members of the Hyades MG, 2MASS J03341065−2130343 of the IC2391 MG, LP 944−20 of the Castor MG and HB 2124−4228 of the Pleiades MG, DENIS-P J0021.0−4244 is a possible member of the IC2391 or Hyades MGs. We discuss our kinematic members below.

4.3.1 LP 944−20

LP 944−20 (BRI 0337−3535) is a nearby (5 pc; Dahn et al. 2002) late M dwarf first identified by Luyten & Kowal (1975). Spectroscopic observations (Tinney 1998) give a spectral type of M9, a v_{rad} of 10 ± 2 km s^{-1}, and place age constraints (using the lithium test; Magazzu, Martín & Rebolo 1993) of ∼475–650 Myr, suggesting a mass range ∼0.056–0.064 $M_\odot$. It is well observed at different wavelengths (e.g. Cushing, Rayner & Vacca 2005), with flaring X-ray emission detected (Rutledge et al. 2000), mid-IR emission measured (Apai et al. 2002), and both flaring and quiescent radio emission detected with the Very Large Array (Berger et al. 2001). Recent spectroscopic analysis measures $v_{rot} \sin i = 30$ km s^{-1} (Zapatero Osorio et al. 2006), and shows a stable v_{rad} over a 6 d period, with no sign of close companions (Martín et al. 2006).

The measured parallax distance and v_{rad} allow accurate *UVW* to be calculated, which are plotted in Figs 7 and 8. Its position in these figures clearly supports its membership of the Castor MG – it lies very close to the canonical *UV* space motion of this group, and is also consistent with this group's *VW* space motion. Our analysis is entirely consistent with Ribas (2003), who previously identified LP 944−20 as a likely member of the Castor MG. As a group member, the age of LP 944−20 would be ∼320 Myr, which is reasonably consistent with the independently determined lithium age constraints. The metallicity could also be inferred as [M/H] = 0.00 ± 0.04 from

Table 3. Spectral ratios for the FEROS objects with corresponding spectral types shown in parentheses.

Name	SpT (lit.)	TiO1+TiO2	VO1+VO2	VO	VO-a	TiO5	SpT (adopt.)
DENIS 004135.3−562112	M7.5[a]	3.33 (M6.0)	–	–	–	0.36 (M8.5)	M7.5
2MASS J03341065−2130343	M6.0[b]	2.78 (M5.0)	–	–	1.98 (M4.5)	0.34 (M4.5)	M4.5
LP 944−20	M9.0[c]	3.16 (M9.0)	3.04 (M8.5)	–	2.28 (M7.5)	0.52 (M9.0)	M8.5
2MASS J04291842−3123568	M7.5/L1 bin.[d]	3.45 (M6.5)	3.08 (M8.0)	–	–	0.20 (M6.0)	M7.0
DENIS 125052.6−212113	M7.5[e]	3.64 (M8.0)	3.06 (M8.5)	–	2.16 (M6.5)	0.18 (M6.5)	M7.5
2MASS J15072779−2000431	M7.5[b]	3.56 (M6.5)	2.67 (M7.0)	1.11 (M8.0)	2.37 (M8.5)	0.15 (M6.5)	M7.5
SIPS 2049−1716	M6.0[f]	3.06 (M5.5)	2.42 (M6.0)	1.08 (M8.0)	2.30 (M8.0)	0.20 (M6.0)	M6.5
SIPS 2128−3254	–	3.13 (M6.0)	2.56 (M6.5)	1.06 (M7.0)	2.18 (M6.5)	0.24 (M5.5)	M6.5

Note. Adopted spectral types are assessing the full range of ratio information available (see text). Literature spectral types are included where available. [a]Phan-Bao & Bessel (2006), [b]Cruz et al. (2003), [c]Tinney (1998), [d]Siegler et al. (2005), [e]Lodieu et al. (2005) and [f]Crifo et al. (2005).

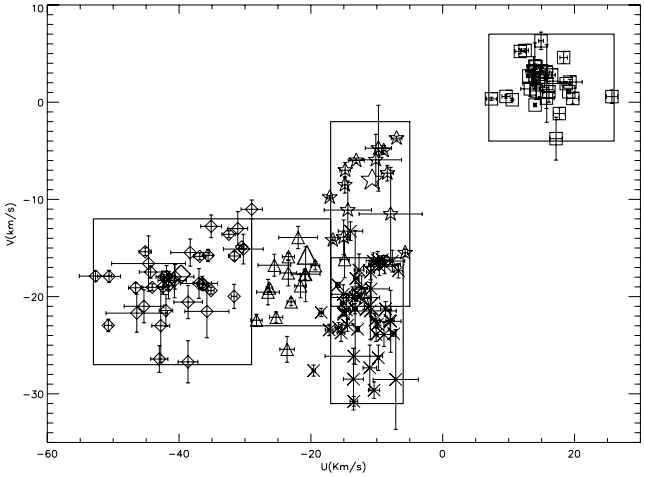

Figure 5. *V* versus *U* space motions of samples of higher mass canonical MG members from the literature (Leggett 1992; Dahn et al. 2002; Knapp et al. 2004; Vrba et al. 2004). The MG regions defined using the samples of higher mass members (see text) are indicated with boxes. We plot members of the Castor, Sirius, Pleiades, IC2391 and Hyades MGs as stars, squares, crosses, triangles and diamonds, respectively. Representative MG space motions (from Table 1) are also plotted for each group as larger symbols of the same type.

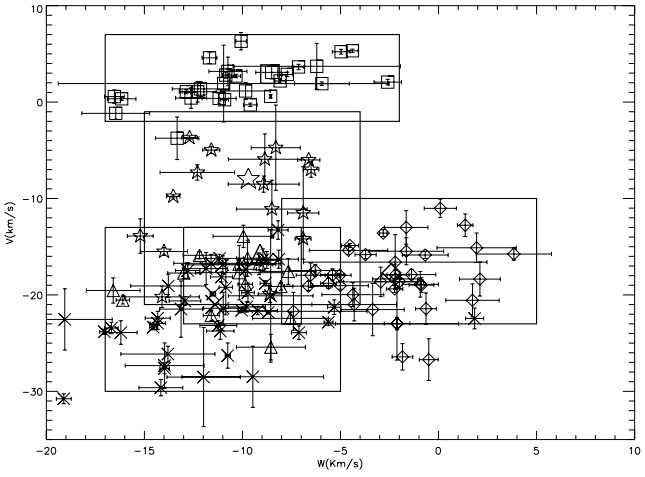

Figure 6. The same as Fig. 5, except showing *V* versus *W* space motions.

Table 1, and the mass (from theoretical models for the assumed Castor age) as 0.063 $M_{\odot}$ (see Ribas 2003). It should be noted that although these models act as a guide, they are subject to significant uncertainties due to minimal consideration of dust opacity. Temperatures can differ by ∼400 K as shown by fig. 1 in Lawson & Feigelson (2001), with models from Baraffe et al. (1998) and Siess, Dufour & Forestini (2000) appearing comparatively cooler. As a result of these known uncertainties note that our mass estimates (particularly those for the youngest candidates) come with the caveat that they could be subject to significant uncertainty, at the level of ∼30–80 per cent for ages from ∼600 Myr down to ∼50 Myr.

4.3.2 DENIS-P J0021.0−4244

DENIS-P J0021.0−4244 (DENIS 0021 hereafter) was first spectral typed by Tinney & Reid (1998), who estimated ≥M9 from low-resolution optical spectroscopy. IR $H-K$ spectroscopy was soon after presented by Delfosse et al. (1999). Basri et al. (2000) list it as an M9.5 dwarf, and use high-resolution Cs I and Rb I spectra to estimate $T_{\rm eff}$ = 2300–2500 K, $v_{\rm rot}\sin i$ = 17.5 km s^{-1} and $v_{\rm rad}$ = 2 ± 1 km s^{-1}. Mohanty & Basri (2003) also present a modest Hα EW of 0.5 Å. Of particular interest is additional spectroscopy in Basri & Reiners (2006) suggesting that DENIS 0021 could have radial velocity variations of 3.0 ± 0.9 km s^{-1} (at the 2σ level), and might thus be a spectroscopic binary.

Using the M_J-spectral type relation from Dahn et al. (2002) with correction for youth, we obtained distance estimates of 23, 26 and 35 pc for the Hyades, Castor and IC2391 MGs, respectively.

Distance and radial velocity estimates show the object to be a possible kinematic member of the IC2391 or Hyades groups. There is some ambiguity to this object's kinematic membership, however, as the space motions that are calculated assuming a young object (∼50 Myr) give a space motion that is more consistent with the relatively older Hyades MG (∼600 Myr). Similarly, the space motions calculated assuming the object is a field dwarf place the object within the selection area of the younger IC2391 MG. However, recalculating space motions assuming DENIS 0021 to be a spectroscopic binary (Object 2 on Figs 7 and 8; see also Table 4), we find it has kinematic membership of IC2391 but no longer of the Hyades MG. To determine the object's membership further follow-up is required (see Section 4.4.2).

4.3.3 HB 2124−4228

Discovered by Hawkins & Bessell (1988), HB 2124−4228 (hereafter HB 2124) is an M8.5 dwarf (Burgasser et al. 2002), with a measured parallax of 28 ± 6 mas yr^{-1} (Tinney 1996, see also Ianna 1993; van Altena, Lee & Hoffleit 1995) putting it at a distance of 36^{+10}_{-7} pc and having $v_{\rm rad}$ = −5.0 ± 3.4 km s^{-1} (Tinney & Reid

Table 4. Radial velocities and derived *UVW* space motions of 10 candidates from the MG candidate member list.

Name	V_{rad} (km s^{-1})	distance (pc)[f]	U (km s^{-1})	V (km s^{-1})	W (km s^{-1})	Moving group candidate
DENIS-P J0021.0−4244	2.0[a] ± 3.0[b]	**35.13 ± 4.28**	$\mathbf{-36.0^{9.7}_{10.9}}$	$\mathbf{-24.2^{8.0}_{9.2}}$	$\mathbf{-6.3^{4.7}_{5.0}}$	**IC2391**
		26.170 ± 3.19	$-26.7^{7.4}_{8.3}$	$-18.1^{6.1}_{7.0}$	$-5.2^{4.2}_{4.5}$	Castor
		23.00 ± 2.80	$\mathbf{-23.4^{6.6}_{7.4}}$	$\mathbf{-15.9^{5.4}_{6.2}}$	$\mathbf{-4.8^{4.1}_{4.3}}$	**Hyades**
DENIS-P J0021.0−4244 (binary corr.)	2.0[a] ± 3.0[b]	**24.90 ± 4.28**	$\mathbf{-25.4^{8.2}_{9.4}}$	$\mathbf{-17.2^{6.5}_{7.7}}$	$\mathbf{-5.0^{4.3}_{4.6}}$	**IC2391**
		18.54 ± 3.19	$-18.8^{6.2}_{7.2}$	$-12.9^{4.9}_{5.9}$	$-4.2^{3.9}_{4.2}$	Castor
		16.30 ± 2.80	$-16.5^{5.6}_{6.4}$	$-11.4^{4.4}_{5.2}$	$-3.9^{3.8}_{4.0}$	Hyades
DENIS-P J004135.3−562112	2.4 ± 1.0	20.80 ± 2.32	$-4.3^{2.5}_{2.9}$	$-10.3^{3.1}_{3.6}$	$0.6^{2.1}_{1.9}$	Pleiades
		18.03 ± 2.01	$-3.6^{2.2}_{2.6}$	$-9.1^{2.8}_{3.1}$	$0.2^{1.9}_{1.8}$	Castor
		18.03 ± 2.01	$-3.6^{2.2}_{2.6}$	$-9.1^{2.8}_{3.1}$	$0.2^{1.9}_{1.8}$	Sirius
2MASS J03341065−2130343	19.0 ± 0.8	**34.94 ± 7.29**	$\mathbf{-20.2^{4.8}_{6.0}}$	$\mathbf{-19.1^{5.4}_{6.7}}$	$\mathbf{-3.0^{5.3}_{4.5}}$	**IC2391**
LP 944−20	10.0 ± 2.0[c]	**5.04 ± 0.11**[d]	$\mathbf{-12.6^{1.4}_{1.5}}$	$\mathbf{-6.9^{1.6}_{1.6}}$	$\mathbf{-3.1^{2.0}_{2.0}}$	**Castor**
2MASS J04291842−3123568	41.9 ± 0.9	16.28 ± 2.22	$-25.9^{2.6}_{3.0}$	$-26.5^{2.1}_{2.5}$	$-21.9^{2.7}_{2.4}$	IC2391
		12.13 ± 1.65	$-24.1^{2.0}_{2.4}$	$-25.9^{1.7}_{2.0}$	$-23.6^{2.2}_{1.9}$	Castor
DENIS-P J125052.6−212113	−7.6 ± 0.4	14.37 ± 1.60	$30.9^{5.5}_{5.2}$	$9.5^{2.2}_{1.9}$	$-21.3^{2.8}_{3.0}$	Pleiades
2MASS J15072779−2000431	−22.2 ± 1.3	18.53 ± 2.06	$-10.6^{3.0}_{2.8}$	$7.9^{2.6}_{2.2}$	$-21.5^{3.2}_{3.6}$	Pleiades
		16.06 ± 1.79	$-11.6^{2.7}_{2.5}$	$7.7^{2.3}_{2.0}$	$-20.2^{2.9}_{3.2}$	Castor
		16.06 ± 1.79	$-11.6^{2.7}_{2.5}$	$7.7^{2.3}_{2.0}$	$-20.2^{2.9}_{3.2}$	Sirius
		14.12 ± 1.57	$-12.3^{2.5}_{2.4}$	$7.4^{2.1}_{1.8}$	$-19.2^{2.6}_{2.9}$	Hyades
SIPS 2049−1716	−35.4 ± 2.4	28.54 ± 4.81	$-51.6^{9.5}_{10.9}$	$-28.8^{5.3}_{6.1}$	$-24.8^{12.9}_{14.6}$	IC2391
		18.68 ± 3.15	$\mathbf{-42.6^{6.8}_{7.8}}$	$\mathbf{-23.9^{3.8}_{4.3}}$	$\mathbf{-9.5^{8.9}_{10.0}}$	**Hyades**
HB 2124−4228	−5.0 ± 3.4[e]	**35.70 ± 10.10**[e]	$\mathbf{-14.6^{8.8}_{11.5}}$	$\mathbf{-29.4^{12.5}_{15.8}}$	$\mathbf{-6.6^{8.6}_{11.2}}$	**Pleiades**
SIPS 2128−3254	−19.8 ± 2.2	**16.61 ± 2.80**	$\mathbf{-30.8^{5.2}_{5.6}}$	$\mathbf{-17.1^{3.7}_{4.1}}$	$\mathbf{-5.1^{5.6}_{5.9}}$	**Hyades**

Note. Rows shown in bold are adopted figures for that object due to kinematic results.
[a]Basri et al. (2000), [b]Basri & Reiners (2006), [c]Tinney (1998), [d]Tinney (1996), [e]Tinney & Reid (1998) and [f] spectroscopic distances unless indicated.

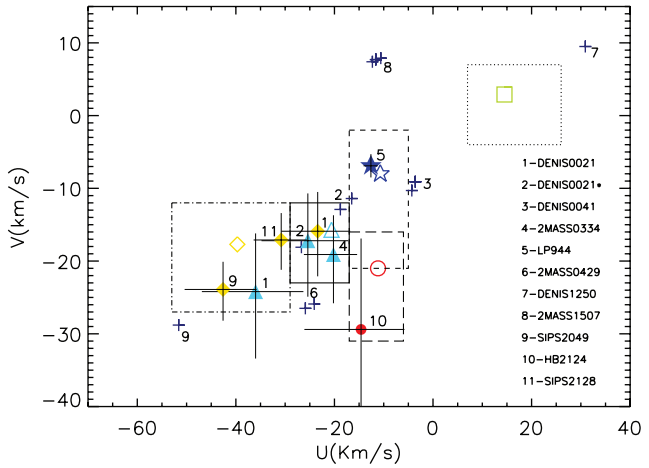

Figure 7. *V* versus *U* space motions of the 10 MG candidates with radial velocities from our observations with FEROS and from the literature plotted as symbols corresponding to their kinematic membership. Space motions that represent membership and non-membership are labelled with the respective object. DENIS 0021 is plotted twice assuming it is a lone object (object 1) and corrected for binarity (see Section 4.3.2; object 2).

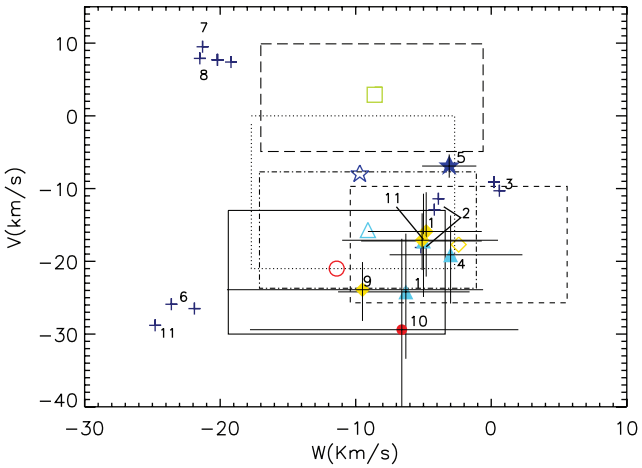

Figure 8. The same as Fig. 7, except showing *V* versus *W*.

1998). The derived *UVW* values are given in Table 4 and plotted in Figs 7 and 8. We note that our value for *V* differs significantly from that presented by Tinney & Reid (1998), who also derived space motions (albeit corrected slightly for solar motion) for this target. In addition, the v_{tan} listed in Tinney & Reid (1998) is too high by comparison with the proper motion and the parallax, thus we will use the *UVW* values defined in this paper.

Photometric and astrometric selection placed this object as a candidate of the Pleiades MG and its space motions confirm kinematic membership. If HB 2124 is a member of the Pleiades MG, its age of 20–150 Myr would give a mass of ∼0.015–0.050 $M_{\odot}$.

4.3.4 2MASS J03341065−2130343

Cruz et al. (2003) found this object to be an M6 dwarf. We find this object to have a spectral type of M4.5 which shows some deviation

from the Cruz value likely due to few usable indices for this object. For this reason, we use the Cruz spectral type when calculating space motions. Correcting for youth to assume an IC2391 membership we estimate the object to have a distance of 34.9 ± 7.3 pc and space motions that confirm kinematic membership. An IC2391 age would suggest a mass of ∼0.075 $M_{\odot}$.

4.3.5 SIPS 2049−1716

SIPS 2049−1716 is an unstudied object that photometric and astrometric tests suggest to be a Hyades candidate, thus inferring a distance estimate of 18.7 ± 3.2 pc. Galactic space motions confirm kinematic membership which would suggest a mass >0.080 $M_{\odot}$.

4.3.6 SIPS 2128−3254

SIPS 2128−3254 is also unstudied. Galactic space motions consistent with a distance estimate of 16.6 ± 2.8 pc show the object to be a kinematic member of the Hyades, which, if confirmed we could infer a mass >0.080 $M_{\odot}$.

4.4 Future follow-up and additional age constraints

4.4.1 Age determination

To obtain radial velocities that are accurate to 1 km s^{-1}, it will be necessary to use high-resolution spectroscopy ($R \sim 30\,000$). This can be done optically in the *I*-band as well as the IR as a high proportion of flux is emitted in these wavebands. Table 5 shows the faintness magnitude limits for the planned spectroscopic follow-up. For high-resolution optical and IR spectroscopic follow-up, the faintness magnitude limits encompass all our MG candidates.

Although radial velocities can constrain our space motions enough to confirm kinematic members of our groups, determination of a candidate's age can finalize its group membership. This can be achieved in such ways as: measurement of the lithium 6708 Å doublet (e.g. Rebolo et al. 1996; Pavlenko et al. 2007); determining rotational velocities to differentiate between young and older M type ultracool dwarf populations (Reiners & Basri 2008); using gravity sensitive spectroscopic features to distinguish between young and old ultracool dwarfs (Gorlova et al. 2004; McGovern et al. 2004); activity/age relation for late-type stars up to a spectral type of M7 (Mochnacki et al. 2002; Silvestri et al. 2006; Reiners & Basri 2008).

Lithium absorption features are much less prominent in late M type objects than in L dwarfs, so intermediate-resolution ($R \geq 8000$) optical spectra will be required for the majority of our candidates (Manzi et al. 2008). At this resolution, we can also measure rotational velocities by measuring the broadening of absorption features.

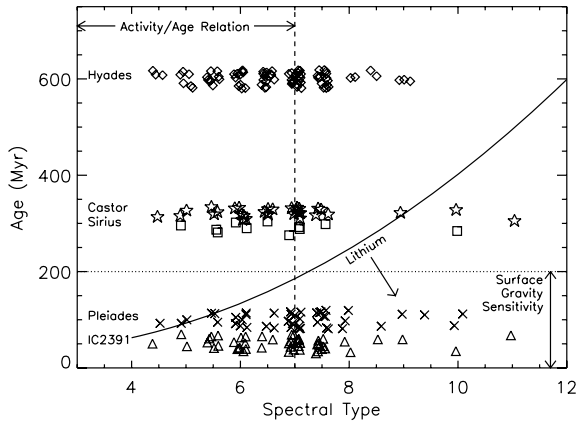

Figure 9. Figure showing age versus spectral type for the candidates along with approximate follow-up limits. The solid line marks the lithium edge with lithium depleted objects to the left. The dashed line marks the limit of age/activity relation studies where objects to the left are plausible for testing. The dotted line represents the upper age limit of testing for MG membership by gravity sensitive spectral features. We plot members of the Castor, Sirius, Pleiades, IC2391 and Hyades MGs as stars, squares, crosses, triangles and diamonds, respectively.

Our three L dwarfs will require only low-resolution spectra ($R \sim 500$) with a good S/N to make lithium observations (Kirkpatrick et al. 1999). This resolution can also provide gravity sensitive and activity/age relation constraints both for the late M and L dwarfs of our sample.

Fig. 9 shows a plot of age (based upon potential group membership) versus spectral type (from Table 2) for our candidates. The figure illustrates which objects would be selected for the various methods of follow-up mentioned previously. Candidates that appear to the right of the lithium edge can be followed up with a lithium test programme, we have 51 objects that qualify for this. There are also 51 candidates that appear younger than 200 Myr, so are eligible for follow-up using spectroscopic gravity sensitive features. We have 93 candidates left of the spectral type = M7 limit and would thus be suitable for age/activity relation follow-up, although candidates with a spectral type close to M7 may be subject to large uncertainties on their age. Of our complete candidate list, we have 23 objects that cannot be tested by any of these methods but will be eligible for age testing using rotational velocities. Rotational velocities could also be used as an extra age constraint for the whole of our candidate list (see Jenkins et al. 2009). Using spectroscopic methods, we can apply at least one non-kinematic test to all our MG candidate providing a solid sample of MG members.

Table 5. Approximate magnitude limits for different spectroscopic resolutions and wavebands are shown, with the potential applications of such spectroscopy for the specified S/N.

Resolution	Waveband	Primary applications	S/N required	*I* limit	*J* limit
High	Optical	Radial velocities	15	18.0	–
	infrared	Radial velocities	15	–	14.5
Intermediate	Optical	Li detection, rotational velocities	30	18.0	–
	infrared	Rotational velocities	30	–	14.5
Low	Optical	Activity/age relation, g sensitivity, Li detection (L dwarfs only)	50	20.5	–
	infrared	Activity/age relation, g sensitivity	50	–	18.5

Note. Magnitude faintness limits are created assuming 0.8 arcsec seeing and a 2 h exposure on an 8-m class telescope.

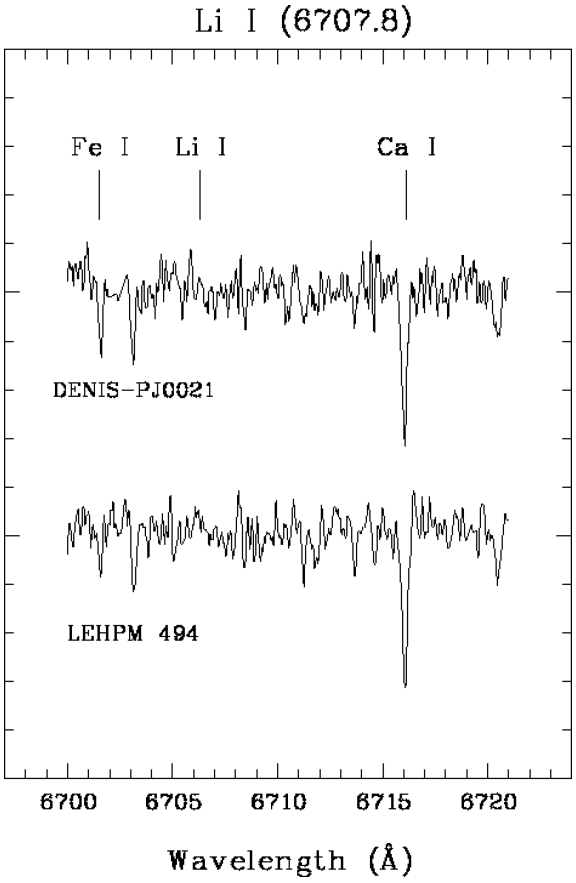

Figure 10. High-resolution spectra obtained using UVES on the VLT for both components of the common proper motion pair DENIS 0021 and LEHPM 494 with a marker showing where the Li I 6707.8 Å absorption line is expected. Other expected feature locations are overplotted.

4.4.2 Lithium detections

Lithium has previously been searched for and detected in LP944−20 (see Section 4.3.1). In order to search for lithium in the ambiguous DENIS 0021, we obtained high-resolution echelle spectra with Ultraviolet and Visual Echelle Spectrograph (UVES) at the ESO VLT-UT2 Kueyen 8-m telescope in 2007 July. We used the UVES standard setting centred on 760 nm, so that the 6707.8 Å lithium absorption line was covered. In this region, the resolution is $R \sim 40\,000$ for a slit width of 1 arcsec. The spectra were extracted using the standard reduction procedures in the IRAF echelle package (bias subtraction, flat-field division and optimal extraction of the spectra). We obtained the wavelength calibration by taking spectra of a Th-Ar lamp. Finally, we corrected from telluric lines and normalized the spectra by a polynomial fit to the observed continuum.

Fig. 10 shows the high-resolution spectra for the lithium region in DENIS 0021 and a common proper motion companion LEHPM 494 found at 78 arcsec (previously discovered by Caballero 2007a,b). Visual inspection clearly reveals the lack of any visible absorption line. Thus, we can say that the objects are either members of the Hyades MG or simply field dwarfs. Improved distance measurements for these objects would further constrain their Galactic space motions. Confirmation of Hyades MG membership would give an age of ∼600 Myr and masses of ∼0.060 and ∼0.095 $M_{\odot}$ for DENIS 0021 and LEHPM 494, respectively.

5 SUMMARY AND FUTURE WORK

We have created a sample of red low-mass objects with proper motions using the ELEHPM and SIPS catalogues. From this, we have found 132 MG candidates using photometric and astrometric techniques. We assess the status of a subset of the catalogue using seven new radial velocities and three from the literature. SIPS 2049−1716 and SIPS 2128−3254 are found to be kinematic members of the Hyades MG, 2MASS J03341065−2130343 of the IC2391 MG, LP 944−20 of the Castor MG and HB 2124−4228 of the Pleiades MG. We find DENIS 0021 to be a possible kinematic member of the Hyades MGs after finding no evidence for lithium absorption within the object's spectra.

The main tool for future work with our MG candidate sample will be the comprehensive measurement of radial velocities, to place accurate constraints on the space motions of the candidates, and identify bona fide kinematic members of the five MGs under consideration. Additional spectroscopic analysis would also be desirable to place direct age constraints on kinematic members, such as the lithium test for the younger group candidates, the study of surface gravity sensitive spectral features, rotational velocities and chromospheric activity (e.g. Gálvez et al. 2006, 2007). Such studies should produce a robust sample of up to ∼75 MG members (see Section 3.4), representing a major new sample of young nearby ultracool dwarfs with well constrained ages and compositions.

This sample could form the basis for studies of low-gravity ultracool atmospheres and low-mass binary systems, as well as providing ideal targets for AO imaging searches for giant extra-solar planets, and further prospects of ultracool dwarf multiple planet systems via future near-IR radial velocity surveys (e.g. Jones et al. 2008).

ACKNOWLEDGMENTS

We acknowledge support from STFC for this work. This research has made use of the SIMBAD database, operated at CDS, Strasbourg, France. We also make use of data products from the Two Micron All Sky Survey, which is a joint project of the University of Massachusetts and the Infrared Processing and Analysis Center/California Institute of Technology, funded by the National Aeronautics and Space Administration and the National Science Foundation.

REFERENCES

Apai D. et al., 2002, ApJ, 573, L115
Asiain R., Figueras F., Torra J., 2000, Ap&SS, 272, 105
Bannister N. P., Jameson R. F., 2005, Astron. Nachr., 326, 1020
Baraffe I., Chabrier G., Allard F., Hauschildt P. H., 1998, A&A, 337, 403
Barrado Y Navacués D., 1998, A&A, 339, 891
Barrado Y Navacués D., 2006, A&A, 459, 511
Basri G., Reiners A., 2006, AJ, 132, 663
Basri G., Mohanty S., Allard F., Hauschildt P. H., Delfosse X., Martín E. L., Forveille T., Goldman B., 2000, ApJ, 538, 363
Berger E. et al., 2001, Nat, 410, 338B
Biller B. A. et al., 2006, ApJ, 647, 464
Boesgaard A. M., Friel E. D., 1990, ApJ, 351, 467
Burgasser A. J., 2004, ApJS, 155, 191
Burgasser A. J., McElwain M. W., 2006, AJ, 131, 1007
Burgasser A. J. et al., 2002, ApJ, 564, 421
Caballero J. A., 2007a, A&A, 462, L61
Caballero J. A., 2007b, ApJ, 667, 520
Chauvin G. et al., 2004, A&A, 425, L29
Costa E. et al., 2005, AJ, 130, 337
Costa E., Mendez R. A., Jao W.-C., Henry T. J., Subasavage J. P., Ianna P. A., 2006, AJ, 132, 1234

Crifo F., Phan-bao N., Delfosse X., Forveille T., Guilbert J., Martín E. L., Reylé C., 2005, A&A, 441, 653
Cruz K. L., Reid I. N., 2002, AJ, 123, 2828
Cruz K. L., Reid I. N., Liebert J., Kirkpatrick J. D., Lowrance P. J., 2003, AJ, 126, 2421
Cushing M. C., Rayner J. T., Vacca W. D., 2005, ApJ, 623, 1115
Dahn C. C. et al., 2002, AJ, 124, 1170
Dehnan W., 1998, AJ, 115, 2384
Delfosse X. et al., 1999, A&AS, 135, 41
De Silva G. M., Sneden C., Paulson D. B., Asplund M., Bland-Hawthorn J., Bessell M. S., Freeman K. C., 2006, AJ, 131, 455
Deacon N. R., Hambly N. C., 2006, MNRAS, 371, 1722
Deacon N. R., Hambly N. C., 2007, A&A, 468, 163
Deacon N. R., Hambly N. C., Cooke J. A., 2005, A&A, 435, 363
De Simone R., Xiaoan W., Tremaine S., 2004, MNRAS, 350, 627
Delgado-Donate E. J., Clarke C. J., Bate M. R., Hodgkin S. T., 2004, MNRAS, 351, 617
Eggen O. J., 1958, MNRAS, 118, 65
Eggen O. J., 1983a, AJ, 88, 190
Eggen O. J., 1983b, AJ, 88, 642
Eggen O. J., 1991, AJ, 102, 2028
Epchtein N. et al., 1997, The Messenger, 87, 27
Faherty J. J., Burgasser A. J., Cruz K. L., Shara M. M., Walter F. M., Gelino C. R., 2009, AJ, 137, 1
Feigelson E. D., Lawson W. A., Stark M., Townsley L., Garmire G. P., 2006, AJ, 131, 1730
Feltzing S., Holmberg J., 2000, A&A, 357, 153
Gálvez M. C., Montes D., Fernández-Figuero M. J., López-Santiago J., 2006, Ap&SS, 304, 59
Gálvez M. C., Montes D., Fernández-Figueroa M. J., de Castro E., Cornide M., 2007, A&A, 472, 587
Gizis J. E., 2002, ApJ, 575, 484
Gorlova N. et al., 2004, ApJS, 154, 448G
Guenther E. W., Torres G., Batalha N., Joergens V., Neuhäuser R., Vijapurker J., Mundt R., 2001, A&A, 366, 965
Hambly N. C., Irwin M. J., MacGillivray H. T., 2001, MNRAS, 326, 1295
Hawkins M. R. S., Bessell M. S., 1988, MNRAS, 234, 177
Ianna P. A., 1993, IAU Symp., 156, 75
Jenkins J. S., Ramsey L. W., Jones H. R. A., Pavlenko Y., Gallardo J., Barnes J. R., Pinfield D. J., 2009, ApJ, 704, 975
Johnson D. R. H., Soderblom D. R., 1987, AJ, 93, 864
Jones H. R. A., Tsuji T., 1997, ApJ, 480, L39
Jones H. R. A. et al., 2008, Proc. SPIE, 7014, 31
Just A., 2003, Ap&SS, 284, 727
Kaufer A., Wolf B., Anderson J., Pasquini L., 1997, ESO Messenger, 89, 8
Kenworthy M. et al., 2001, ApJ, 554, 67
King J. R., Schuler S. C., 2005, PASP, 117, 911
King J. R., Villarreal A. R., Soderblom D. R., Gulliver A. F., Adelman S. J., 2003, AJ, 125, 1980
Kirkpatrick J. D., Henry T. J., McCarthy D. W., 1991, ApJS, 77, 417
Kirkpatrick J. D., Henry T. J., Simons D. A., 1995, AJ, 109, 797
Kirkpatrick J. D. et al., 1999, ApJ, 519, 802
Kirkpatrick J. D. et al., 2000, AJ, 120, 447
Kirkpatrick J. D., Barman T. S., Burgasser A. J., McGovern M. R., McLean I. S., Tinney C. G., Lowrance P. J., 2006, ApJ, 639, 1120
Knapp G. R. et al., 2004, AJ, 127, 3553
Kroupa P., Aarseth S., Hurley J., 2001, MNRAS, 321, 699
Lawson W. A., Feigelson E. D., 2001, in Montmerle T., André P., eds, ASP Conf. Ser. Vol. 243, From Darkness to Light. Astron. Soc. Pac., San Francisco, p. 591
Leggett S. K., 1992, ApJS, 82, 351
Leggett S. K., Allard F., Hauschildt P. H., 1998, ApJ, 509, 836
Lépine S., 2005, AJ, 130, 1247
Lépine S., Shara M. M., Rich R. M., 2002, AJ, 124, 1190
Lodieu N., Scholz R.-D., McCaughrean M. J., Ibata R., Irwin M Z. H., 2005, A&A, 440, 1061
Lodieu N., Hambly N. C., Jameson R. F., Hodgkin S. T., 2008, MNRAS, 383, 1385
López-Santiago J., Montes D., Crespo-Chacón I., Fernández-Figueroa M. J., 2006, ApJ, 643, 1160
Luhman K. L., 2004, ApJ, 614, 398
Luhman K. L., McLeod K. K., Goldenson N., 2005, ApJ, 623, 1141
Luyten W. J., Kowal C. T., 1975, A Catalogue of Stars with Proper Motions Exceeding 0.5″ Annually. Univ. Minnesota Press, Minneapolis
Magazzu A., Martín E. L., Rebolo R., 1993, ApJ, 404, L17
Makarov V. V., 2003, AJ, 126, 1996
Manzi S., Randich S., de Wit W. J., Palla F., 2008, A&A, 479, 141
Martín E. L., Delfosse X., Basri G., Goldman B., Forveille T., Zapatero Osorio M. R., 1999, AJ, 118, 2466
Martín E. L., Guenther E., Zapatero Osorio M. R., Bouy H., Wainscoat R., 2006, ApJ, 644, L75
McGovern M. R., Kirkpatrick J. D., McLean I. S., Burgasser A. J., Prato L., Lowrance P. J., 2004, ApJ, 600, 1020
Mochnacki S. W. et al., 2002, AJ, 124, 2868
Mohanty S., Basri G., 2003, ApJ, 583, 451
Montes D., López-Santiago J., Gálvez M. C., Fernandez-Figueroa M. J., De Castro E., Cornide M., 2001, MNRAS, 328, 45
Nakajima T. et al., 2005, Astron. Nachr., 326, 952
Nordström B. et al., 2004, A&A, 418, 989
Paulson D. B., Yelda S., 2006, PASP, 118, 706
Paulson D. B., Sneden C., Cochran W. D., 2003, AJ, 125, 3185
Pavlenko Ya. V., Jones H. R. A., Martín E. L., Guenther E., Kenworthy M. A., Zapatero Osorio M. R., 2007, MNRAS, 380, 1285
Phan-Bao N., Bessel M. S., 2006, A&A, 446, 515
Pinfield D. J., Jones H. R. A., Steele I. A., 2005, PASP, 117, 173
Pinfield D. J. et al., 2006, MNRAS, 368, 1281
Pokorny R. S., 2004, Ph.D. thesis, Liverpool John Moores University
Pokorny R. S., Jones H. R. A., Hambly N. C., 2003, A&A, 397, 575
Pokorny R. S., Jones H. R. A., Hambly N. C., Pinfield D. J., 2004, A&A, 421, 763
Randich S., Pallavicini R., Meola G., Stauffer J. R., Balachandran S. C., 2001, A&A, 372, 862
Rebolo R., Martín E. L., Basri G., Marcy G. W., Zapatero-Osorio M. R., 1996, ApJ, 469, L53
Reid N., 1992, MNRAS, 257, 257
Reid I. N. et al., 1999, ApJ, 521, 613
Reiners A., Basri G., 2008, ApJ, 684, 1390
Ribas I., 2003, A&A, 400, 297
Rocha-Pinto H. J., Scalo J., Maciel W. J., Flynn C., 2000, ApJ, 531, L115
Ruiz M. T., Takamiya M. Y., Roth M., 1991, ApJ, 367, L59
Rutledge R. E., Basri G., Martín E. L., Bildsten L., 2000, ApJ, 538, L141
Scholz R.-D., Ibata R., Irwin M., Lehmann I., Salvato M., Schweitzer A., 2002, MNRAS, 329, 109
Siegler N., Close L. M., Cruz K. L., Martín E. L., Reid I. N., 2005, ApJ, 621, 1023
Siess L., Dufour E., Forestini M., 2000, A&A, 358, 593
Silvestri N. M. et al., 2006, AJ, 131, 1674
Soderblom D. R., Mayor M., 1993, AJ, 105, 226
Subasavage J. P., Henry T. J., Hambly N. C., Brown M. A., Jao W.-C., Finch C. T., 2005, AJ, 130, 1658
Taylor B. J., 2000, A&A, 362, 563
Tinney C. G., 1996, MNRAS, 281, 644
Tinney C. G., 1998, MNRAS, 296, L42
Tinney C. G., Reid I. N., 1998, MNRAS, 301, 1031
van Altena W. F., Lee J. T., Hoffleit E. D., 1995, The General Catalogue of Trigonometric Stellar Parallaxes, 4th edn. Yale Univ. Obs., New Haven
Vrba F. J. et al., 2004, AJ, 127, 2948
Whitworth A. P., Stamatellos D., 2006, A&A, 458, 817
Zapatero Osorio M. R., Martín E. L., Bouy H., Tata R., Deshpande R., Wainscoat R. J., 2006, ApJ, 647, 1405
Zuckerman B., Song I., 2004, ARA&A, 42, 685
Zuckerman B., Song I., Bessell M. S., Webb R. A., 2001, ApJ, 562, L87

This paper has been typeset from a TEX/LATEX file prepared by the author.